SYNCHRONIZATION OF NEURAL OSCILLATORS WITH DIFFUSIVE COUPLING: DOES THE LEAKAGE OF NEUROTRANSMITTER MATTER?

D.J. Rijlaarsdam, I. Tyukin, H. Nijmeijer, A. Semyanov, C. van Leeuwen

Abstract— We analyze the dynamics of neural oscillators in the presence of both synaptic and diffusive coupling. First we derive a computationally effective, yet plausible model of extra-synaptic neurotransmitter diffusion. Second, we modify the Hindmarsh-Rose oscillator to account for the diffusion. For ensembles of these modified model neurons we obtain conditions ensuring global synchronization. Our results demonstrate that diffusion substantially affects the dynamics of a network of model neurons.

I. INTRODUCTION

Synaptic signal transmission is traditionally believed to be the principal medium for neural interaction. Recent studies show that spillover of neural transmitters from the synaptic clefts may constitute an additional channel for neural interaction [1], [12], [13]. According to [5], extrasynaptic signalling accounts for up to 75% of interneuronal communication. Despite the fact that these empirical findings have attracted substantial interest worldwide, there are few theoretical studies of neural oscillators that take these observations into account.

In our paper we aim to resolve this problem and provide a theoretical analysis of neural dynamics taking spillover of a neurotransmitter (NT) into account. In order to do this we propose a computationally effective mathematical model

of spillover. We found that transmitter diffusion can be described by time-varying coupling, of which the steady-state solution generally follows a Gaussian law. We implemented this coupling in a Hindmarsh-Rose model neuron and analyzed its effect on the dynamics of single cells and populations. Extrasynaptic diffusion results in a system in which the oscillators are coupled through variables with substantially different time scales. For this new class of systems we derived sufficient conditions for complete synchronization.

The paper is organized as follows: in section II we present a technique, allowing us to model diffusion of neurotransmitter using the photographic images of brain tissue. For the sake of computational effectiveness the model was restricted to the steady-state solutions of the diffusion equation in two spatial dimensions. In section III we analyze how diffusion affects asymptotic properties of ensembles of neural oscillators. In section IV we provide results of simulations and section V concludes the paper.

II. COUPLING BY DIFFUSION

In studying diffusion of neurotransmitter (NT), we must pay attention to the structure of the extracellular matrix (ECM). We provide a technique for reconstructing the topology of the ECM from photographic images. This is necessary for estimating profiles of the NT concentration in the tissue. These profiles are essential in order to derive a model of the diffusive coupling.

Tissue Topology. We derived the profile of the tissue by analyzing a set of photographic images[1] of the hippocampal tissue of an adult mouse (figure 1). The upper part of figure 1a resembles the dendritic area, where spillover of NT is most likely to occur. Hence we restrict our analysis to these areas (see figure 1b, where black areas correspond to obstructions and white areas correspond free

Dept. of Mechanical Engineering, Eindhoven University of Technology, P.O. Box 513 5600 MB, Eindhoven, The Netherlands, (e-mail: d.j.rijlaarsdam@student.tue.nl). Part of this work has been done while the first author was at the RIKEN Brain Science Institute

Dept. of Mathematics, University of Leicester, University Road, Leicester, LE1 7RH, UK (e-mail: I.Tyukin@le.ac.uk); and Laboratory for Perceptual Dynamics, RIKEN Brain Science Institute, Wako-shi, Saitama, 351-0198, Japan;

Dept. of Mechanical Engineering, Eindhoven University of Technology, P.O. Box 513 5600 MB, Eindhoven, The Netherlands, (e-mail: h.nijmeijer@tue.nl)

Neuronal Circuit Mechanisms Research Group, RIKEN Brain Science Institute, Wako-shi, Saitama, 351-0198, Japan (e-mail: semyanov@brain.riken.jp)

Laboratory for Perceptual Dynamics, RIKEN Brain Science Institute, Wako-shi, Saitama, 351-0198, Japan (e-mail: ceesvl@brain.riken.jp)

[1]The images were provided by Dr. S. Grebenyuk, Neuronal Circuit Mechanisms Research Group, RIKEN Brain Science Institute, Wako-shi, Saitama, 351-0198, Japan
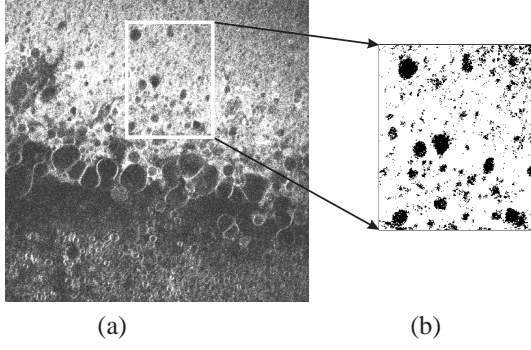
Fig. 1. (a) Photograph of a slice of hippocampal tissue. (b) Dendritic area.

space). We aim to model the tissue ensuring 1) a realistic ratio between the free space and volume occupied by obstructions, and 2) a realistic distribution of sizes of these obstructions. The first characteristic can be estimated explicitly from the images and is generally about 8%. To satisfy the second requirement we must have a model of the most probable shape of an obstructing object. As follows from visual inspection the obstacles have roughly a circular shape.

The probability $\wp(d_j)$ for an obstruction with diameter d_j to exist, is derived from the images by estimating the lengths of black space, row wise in the images. We use these estimates to derive a distribution $\mathfrak{m}(i)$ of occurrences of filled (black) lines with lengths grater or equal than i in the actual images. On the other hand, in each measurement $\mathfrak{m}(i)$ a circular object with diameter $d_j > i$ will be encountered in multiple lines (figure 2). This leads to the following contribution of
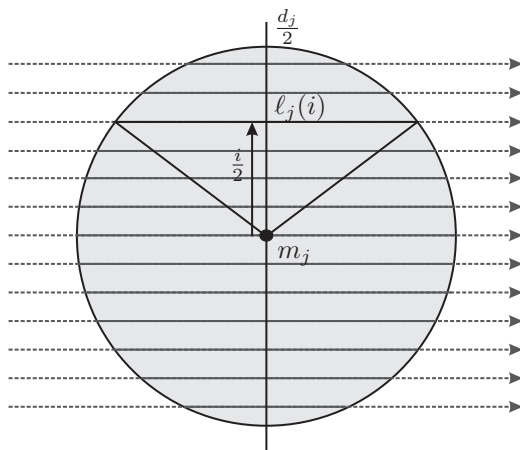
Fig. 2. Contribution of black space in a circle.

lengths $\ell_j(i)$ to $\mathfrak{m}(i)$:

$$\ell_j(i) = \sqrt{d_j^2 - i^2} \qquad \forall\, 0 \le i \le d_j, \qquad (1)$$

where i is the distance to the center m_j of an obstruction. Distributions (1) were fit to $\mathfrak{m}(i)$ according to the following criterion:

$$\min_{\boldsymbol{\alpha}} \left(\mathfrak{m}(i) - \sum_{j=1}^{n} \alpha_j \sqrt{d_j^2 - i^2} \right)^2, \qquad (2)$$

where n is the width of the picture in pixels. The coefficients α_j represent the contribution of circles with diameter d_j. The resulting normalized distribution $\wp(d_j)$ is provided in figure 3. The process is repeated in the vertical direction, column wise (dashed curve). Slight mismatches between the curves in figure 3 are due to the fact that cells are not perfectly circular.
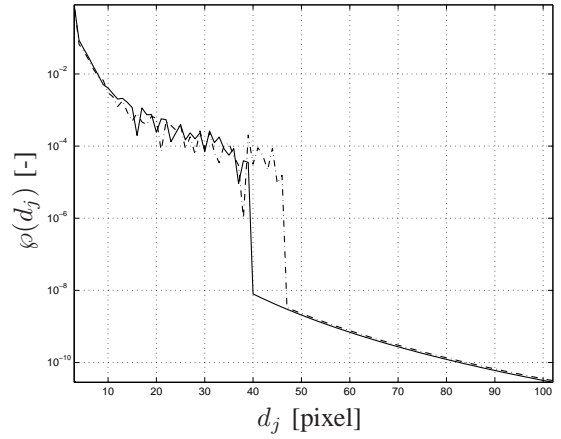
Fig. 3. Probability distribution $\wp(d_j)$ of sizes d_j of obstructing objects in horizontal (solid) and vertial (dashed) directions.

Simulation of Diffusion. The model of hippocampal tissue (distribution $\wp(d_j)$) was used to create a realistic environment for simulating diffusion of the NT. In addition to preserving the ratio between obstructed and free space we also require that cells in this environment do not intersect.

Free diffusion in 2 dimensions is often [9] modeled by the following PDE:

$$\frac{\partial C}{\partial t} = \mathcal{D} \left(\frac{\partial^2 C}{\partial x^2} + \frac{\partial^2 C}{\partial y^2} \right) + u\left(x, y, t\right), \qquad (3)$$

where $x \in \mathbb{R}$, $y \in \mathbb{R}$ are spatial variables, $\mathcal{D} \in \mathbb{R}_{>0}$ is the diffusion coefficient and $u(x,y,t) : \mathbb{R} \times \mathbb{R} \times \mathbb{R}_{>0} \to \mathbb{R}$ represents the input of NT to the system. The function $C(x,y,t) : \mathbb{R} \times \mathbb{R} \times \mathbb{R}_{>0} \to \mathbb{R}$ represents the concentration profile over an open, connected set $\Omega \subset \mathbb{R}^2$. Only time invariant sources are considered, and the boundary conditions are: $C(x,y,t) = 0 \ \forall \ x,y \ne \Omega$.

If Ω inherits structural properties of the tissue then solutions of (3) over Ω would provide realistic estimates of the NT concentration in the actual tissue. We calculate these solutions by approximating original PDE (3) with a system of ODE, subject to accurate spatial discretization over Ω:

$$\dot{\bar{c}} = K\bar{c} + \bar{u}, \qquad (4)$$

where $\bar{c} \in \mathbb{R}^{N^2}$ is a vector formed by spatial sampling of Ω over N^2 patches. The matrix $K \in \mathbb{R}^{N^2 \times N^2}$ is the discrete approximation of the Laplacian [6] in the coordinates of $\bar{c}$:

$$\left.\frac{\partial^2 f}{\partial x^2}\right|_{(m,n)} + \left.\frac{\partial^2 f}{\partial y^2}\right|_{(m,n)} \qquad (5)$$
$$\approx f(m \pm 1, n) + f(m, n \pm 1) - 4f(m, n).$$

Variables $m, n \in \{1, 2, \ldots N\}$ represent the location of the ith cell in the grid. Notice that cells which are (partly) inside obstructions correspond to zero rows and columns in K. Hence, it is enough to consider a reduced matrix $\Pi \in \mathbb{R}^{r^2 \times r^2}$, with r the number of cells that allow for flow of NT. Its properties are summarized below:

Property 1: The reduced coupling matrix
1. Π is symmetric.
2. Π is non-singular, hence Π^{-1} exists.
3. Π is negative definite.

Proof of Property 1 Symmetry of Π follows directly from the rule (5) according to which K and Π are generated. Non-singularity of Π is proven by using the results of Taussky [14]. In this reference it is shown that a matrix $A \in \mathbb{R}^{n \times n}$ with complex elements is nonsingular if 1) A can not be transformed to the form:

$$A = \begin{bmatrix} P & U \\ 0 & Q \end{bmatrix}, \qquad (6)$$

by the same permutation of the rows and columns (P and Q are square matrices and 0 consists of zeros), and 2) its elements A_{ij} satisfy:

$$|A_{ii}| \geq \sum_{k=1,\, k \neq i}^{n} |A_{ik}|, \qquad (7)$$

with inequality in at most $n-1$ cases. Since, Π is generated over a connected set, Π is not reducible to the form (6). Furthermore, Π obeys (7). Hence according to [14], it is non-singular. Then negative definiteness of Π follows from Gershgorins' circle theorem *QED*.

The solution to (4) now reduces to that of:

$$\dot{c} = \Pi c + u \qquad (8)$$

with $c, u \in \mathbb{R}^{r^2}$ and $\Pi \in \mathbb{R}^{r^2 \times r^2}$. Its general form is given by $c(t) = e^{\Pi t}c(0) + \int_0^t e^{\Pi(t-\tau)}u d\tau$.

However, for the sake of simplicity we consider its steady-state component:

$$\lim_{t \to \infty} c(t) = -\Pi^{-1}u. \qquad (9)$$

To complete our derivations of concentration profiles we need to specify the input u.

A neuron consists of a cell body to which an axon and dendrites are attached. Assuming dendrites spread equally in all directions and have a mean length ζ, NT is most probable to be released on and sensed at a circle with radius ζ. From this circle the release power, as well as the receptor sensitivity are assumed to obey a Gaussian law (figure 4). Furthermore, the coupling from
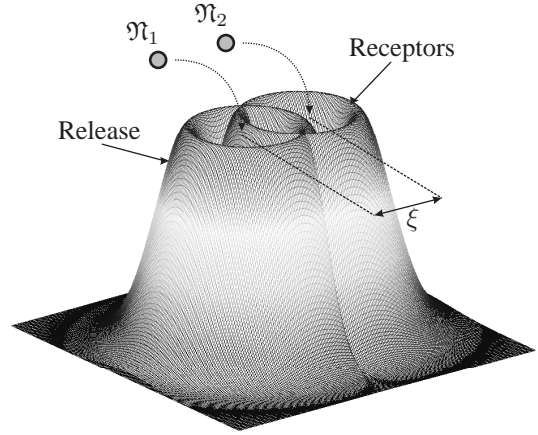
Fig. 4. Schematic depiction of the release power and receptor sensitivity distribution (no obstructions).

one neuron to another is defined as the amount of NT sensed by a neuron. When obstructions are disregarded both the release and the receptor profile can be described by the difference between two Gaussian functions $\mathcal{G}^2(x, y)$ centered around the same mean:

$$\Delta_1(x, y) = \mathcal{G}^2_{\boldsymbol{\mu}_{1,1}, \boldsymbol{\sigma}_{1,1}}(x, y) - \mathcal{G}^2_{\boldsymbol{\mu}_{1,2}, \boldsymbol{\sigma}_{1,2}}(x, y). \qquad (10)$$

The total coupling function is the convolution between these two profiles Δ_1 and Δ_2:

$$\kappa(\xi) = \kappa(x, y) = \Delta_1(x, y) \otimes \Delta_2(x, y), \qquad (11)$$

where $\xi = \|\boldsymbol{\mu}_1 - \boldsymbol{\mu}_2\|$ is the difference between the means of the two Gaussian differences and $\otimes$ is the convolution operator. The convolution (11) possesses the following properties:

Property 2: Coupling function
1. $\kappa(\xi)$ is positive definite.
2. $\kappa(\xi)$ is bounded from above and below by bell

shaped functions.

3. $\kappa(\xi)$ is monotonically increasing for $\xi < 0$ and monotonically decreasing for $\xi > 0$. It therefore possesses a global maximum at $\xi = 0$.

The proof is available in [4].

When obstructions are taken into account, the shape of the coupling function can be obtained by numerical simulation. Results of these simulations, for multiple instances of Ω, are presented in figure 5. These results closely resemble a Gaussian function, as predicted by the analytical estimate before. Therefore, this analysis suggests the Gaussian function as a plausible model for the diffusive coupling.
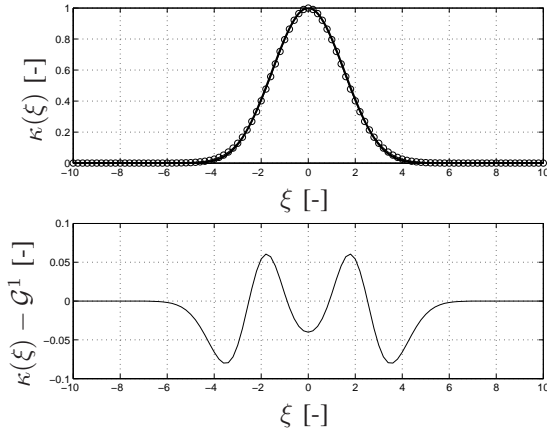
Fig. 5. Numerical approximation of the coupling function $\kappa(\xi)$. Top figure: simulation results (-), Gaussian fit (o-). Lower figure: error.

III. Dynamics of Neuronal Oscillators with Diffusive and Synaptic Coupling

In section II we obtained a plausible class of diffusive coupling functions $\kappa(\xi)$ (11). Here we study the dynamics of neural ensembles taking this coupling into account. We consider a network of Hindmarsh-Rose (1989) model neurons [10]. These model neurons are computationally effective, cover substantially large variety of neural behavior [8], and can be fitted successfully to actual data [7].

The 1989 Hindmarsh & Rose Model Revisited. In order to take diffusion of neurotransmitter into account we extend the original Hindmarsh & Rose model by adding an extra 'diffusion' component. This addition should, however, satisfy the following constraints: 1. it should be a Gaussian function $\kappa(\xi)$ of the distance between the neurons 2. it should contain a time varying component on a timescale that is much slower than those present in the current model. Summarizing, the

i^{th} component in the new model consisting of n diffusively coupled neurons is defined as follows:

$$\dot{x}_i = -ax_i^3 + bx_i^2 + y_i - z_i + I \quad (12)$$
$$\quad - \ \mathbf{\Gamma}_{s_i}\mathbf{x} + \mathbf{D}_i\mathbf{q}$$
$$\dot{y}_i = c - dx_i^2 - y_i \quad (13)$$
$$\dot{z}_i = \varepsilon\left(s\left(x_i + x_0\right) - z_i\right) \quad (14)$$
$$\dot{q}_i = \tau_q^{-1}\left(x_i + \vartheta - kq_i\right), \quad (15)$$

where a, b, c, ε, s, k, $\tau_q \in \mathbb{R}_{>0}$ are the model parameters, and the function of parameter $\vartheta \in \mathbb{R}_{>0}$ ensures $x_i(t) + \vartheta > 0 \ \forall \ t \in \mathbb{R}_{\geq 0}, i = 1, 2, \dots, n$. I is an external current, and $\mathbf{x} = (x_1, \dots, x_n)^T$, $\mathbf{q} = (q_1, \dots, q_n)^T$. Synaptic coupling is modeled by a linear term $\mathbf{\Gamma}_{s_i}\mathbf{x}$, with $\mathbf{\Gamma}_{s_{ij}} = -k_s \ \forall \ i \neq j$ and $\mathbf{\Gamma}_{s_{ii}} = k_s(n-1)$. Here, $\mathbf{\Gamma}_s \geq 0$ and $k_s \in \mathbb{R}_{\geq 0}$ is a synaptic gain. Diffusive coupling is represented by $\mathbf{D}_i\mathbf{q}$, with $\mathbf{D}_{ij} = k_d\kappa\left(\xi_{ij}\right)$. Here, $\mathbf{D} = \mathbf{D}^T$, $k_d \in \mathbb{R}_{\geq 0}$ is a diffusive gain and $\kappa(\xi)$ is a Gaussian coupling function, as derived in (11).

Asymptotic Properties of the Model. Equations (12) - (15) define the dynamics of model neurons that are both diffusively and synaptically coupled. In contrast to the original Hindmarsh & Rose model, the new model possesses three instead of two different timescales. In addition, as a result of slow diffusion, neurons themselves interact at different time scales. These properties might affect asymptotic behavior of the ensembles. Here we investigate these properties from the point of view of synchronization. Following [15], we derive the following properties:

Property 3: Consider diffusively coupled system (12) - (15)

1. Its solutions are globally bounded.

2. The diagonal synchronization manifold $\mathbf{x}_1 = \mathbf{x}_2 = \dots = \mathbf{x}_n$, $\mathbf{x}_i = (x_i, y_i, z_i, q_i)$ is globally asymptotically stable if:

$$k_s > \frac{\frac{1}{2}d^2 + b^2}{n} \text{ and } \mathbf{\Xi} \leq 0, \quad (16)$$

with:

$$\mathbf{\Xi} = \left[\begin{array}{c|c} -\gamma\mathbf{C}_x & \mathbf{C}_x\mathbf{D} + \frac{\alpha}{\tau_q}\mathbf{C}_x \\ \hline \mathbf{C}_x\mathbf{D} + \frac{\alpha}{\tau_q}\mathbf{C}_x & -\frac{2\alpha}{\tau_q}k\mathbf{C}_x \end{array}\right],$$

where $\mathbf{C}_x$ only has nonzero elements $\mathbf{C}_{x,ii\pm1} = -1$ and $\mathbf{C}_{x,ii} = 2$, except $\mathbf{C}_{x,11} = \mathbf{C}_{x,nn} = 1$.

$$\gamma = \sum_{i=1}^{n-1}\left(nk_s - \frac{d^2}{2} - b^2\right) \quad , \alpha \in \mathbb{R}_{>0}, \ (17)$$

Proof. Boundedness of solutions follows from the semi-passivity argument [2], [15] using the following storage function:

$$V_i = \frac{1}{2}\left(x_i^2 + y_i^2 + z_i^2 + q_i^2\right), \qquad (18)$$

for the i-th system. Details are provided in [4].

The stability of the synchronization manifold is investigated using the following candidate Lyapunov function:

$$\mathcal{V}_S = \boldsymbol{x}^T \frac{\boldsymbol{C}_x}{c_x}\boldsymbol{x} + \boldsymbol{y}^T\frac{\boldsymbol{C}_y}{c_y}\boldsymbol{y} \qquad (19)$$
$$+\boldsymbol{z}^T\frac{\boldsymbol{C}_z}{c_z}\boldsymbol{z} + \boldsymbol{q}^T\frac{\boldsymbol{C}_q}{c_q}\boldsymbol{q},$$

with $\boldsymbol{C}_y, \boldsymbol{C}_z, \boldsymbol{C}_q$ defined similar to the definition of $\boldsymbol{C}_x$ in property 3, $c_x, c_y, c_z, c_q \in \mathbb{R}_{>0}$. Using results from [15] we find:

$$\dot{\mathcal{V}}_S \leq -\gamma \boldsymbol{x}^T\boldsymbol{C}_x\boldsymbol{x} - \varepsilon \boldsymbol{z}^T\boldsymbol{C}_z\boldsymbol{z} \qquad (20)$$
$$+\boldsymbol{x}^T\boldsymbol{C}_x\boldsymbol{D}\boldsymbol{q} + \boldsymbol{q}^T\boldsymbol{D}^T\boldsymbol{C}_x\boldsymbol{x}$$
$$+\frac{2}{\tau_q}\boldsymbol{q}^T\boldsymbol{C}_q\boldsymbol{x} - \frac{2k}{\tau_q}\boldsymbol{q}^T\boldsymbol{C}_q\boldsymbol{q},$$

with γ according to (17). Now, note the following, regarding equation (20):

- $\gamma > 0 \ \forall \ k_s > \frac{\frac{d^2}{2}+b^2}{n}$ (see (17) and [15]).
- The term $-\varepsilon \boldsymbol{z}^T\boldsymbol{C}_z\boldsymbol{z}$ is disregarded, making the estimate more conservative, but yielding a more compact result.
- Terms involving constants vanish in the derivative because of the structure of $\boldsymbol{C}_i$.

With $\boldsymbol{C}_q = \alpha \boldsymbol{C}_x$, $\alpha \in \mathbb{R}_+$, $\beta = \frac{2}{\tau_q}$ and using the fact that $\boldsymbol{C}_x$ is symmetric, equation (20) can be written as:

$$\dot{\mathcal{V}}_S \leq -\gamma \boldsymbol{x}^T\boldsymbol{C}_x\boldsymbol{x} - \alpha\beta k \boldsymbol{q}^T\boldsymbol{C}_x\boldsymbol{q} \quad (21)$$
$$+\boldsymbol{x}^T\left(2\boldsymbol{C}_x\boldsymbol{D} + \alpha\beta\boldsymbol{C}_x\right)\boldsymbol{q}$$

Or in more compact notation, with $\phi \in [0\ 1]$:

$$\dot{\mathcal{V}}_S \leq \boldsymbol{w}^T\boldsymbol{\Xi}_\phi\boldsymbol{w} \qquad (22)$$
$$-\phi\gamma\boldsymbol{x}^T\boldsymbol{C}_x\boldsymbol{x} - \phi\alpha\beta k\boldsymbol{q}^T\boldsymbol{C}_x\boldsymbol{q}, \ \phi \in [0\ 1]$$

with $\boldsymbol{w} = \begin{bmatrix} \boldsymbol{x} & \boldsymbol{q} \end{bmatrix}^T$ and

$$\boldsymbol{\Xi}_\phi = \left[\begin{array}{c|c} -\gamma(1-\phi)\boldsymbol{C}_x & \boldsymbol{C}_x\boldsymbol{D} + \frac{\alpha\beta}{2}\boldsymbol{C}_x \\ \hline \boldsymbol{C}_x\boldsymbol{D} + \frac{\alpha\beta}{2}\boldsymbol{C}_x & -\alpha\beta k(1-\phi)\boldsymbol{C}_x \end{array} \right].$$

Given that $\boldsymbol{\Xi}_\phi$ is negative semi-definite we can conclude from (22) that $\dot{\mathcal{V}}_S \leq 0$. Therefore, integrals $\int_0^\infty \boldsymbol{x}^T(\tau)\boldsymbol{C}_x\boldsymbol{x}(\tau)d\tau$, $\int_0^\infty \boldsymbol{q}^T(\tau)\boldsymbol{C}_q\boldsymbol{q}(\tau)d\tau$ are bounded. Hence, applying Barbalatt's lemma we can derive that $\boldsymbol{x}^T(t)\boldsymbol{C}_x\boldsymbol{x}(t) \rightarrow 0$, $\boldsymbol{q}^T(t)\boldsymbol{C}_q\boldsymbol{q}(t) \rightarrow 0$ as $t \rightarrow \infty$.

Furthermore, looking at equations (12) - (15) it is observed that if $x_i(t)$ is regarded as a (bounded)

input to this system, which for $t \rightarrow \infty$ is identical for all systems, the resulting system is linear and asymptotically stable. From [3], [11] it is known that any linear and asymptotically stable system is convergent. Hence, $y_i(t)$, $i = 1, \ldots, n$ converge to the same function of time. Therefore, $\boldsymbol{y}^T(t)\boldsymbol{C}_y\boldsymbol{y}(t) \rightarrow 0$ as $t \rightarrow \infty$. Applying the same argument to variables $z_i(t)$ we prove that $\boldsymbol{z}^T(t)\boldsymbol{C}_z\boldsymbol{z}(t) \rightarrow 0$ as $t \rightarrow \infty$.

Therefore it can be concluded that $\boldsymbol{x}(t)$, $\boldsymbol{q}(t)$, $\boldsymbol{y}(t)$ and $\boldsymbol{z}(t)$ converge to the synchronization (diagonal) manifold as $t \rightarrow \infty$ if $\boldsymbol{\Xi} = \boldsymbol{\Xi_0} \leq 0$. *QED*

IV. SIMULATION RESULTS

This section provides two examples demonstrating dynamical regimes inherent to the extended model and not observed in the original Hindmarsh & Rose model.

Saturation. Consider a ring of $n = 5$ synaptically and diffusively coupled modified Hindmarsh & Rose neurons. The neurons are located on a circle with radius 1 and the parameters of the system and coupling strengths are chosen as follows:

$$a = 1, b = 3, c = 1, d = 5, x_0 = 1.618,$$
$$\varepsilon = 0.005, I = 1, \vartheta = 1.6, \tau_q = 100, \qquad (23)$$
$$k_s = 1, k_d = 0.6, k = 0.095, s = 4.$$

Furthermore, the diffusive coupling between the neurons is a Gaussian function with $\sigma = 2$. The effects of diffusive coupling are clearly visible, in the results depicted in figure 6. From figure 6
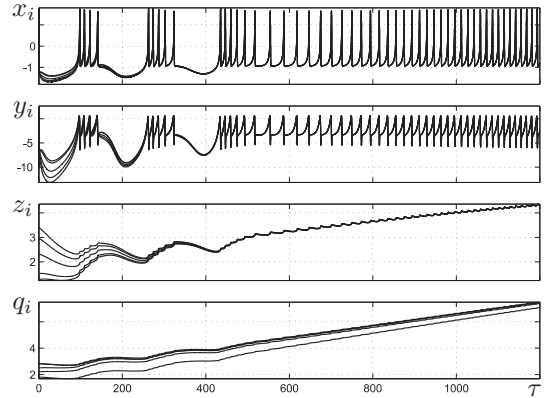
Fig. 6. Simulation results (saturation).

we observe the following: First of all, a dynamic component is observed in both the inter-burst interval (decreasing) and the number of spikes per burst (increasing). Furthermore, we observe the presence of saturation in the systems' dynamics. The timescales in the system have a ratio $x(\tau)$:

$z(\tau) : q(\tau)$ of 5000:10:1. Since the timescale of neuronal spiking $x(\tau)$ is normally in the order of milliseconds, the 'speed' of diffusion $q(\tau)$ is in the order of seconds. Last but not least, it is worth noticing that the parameter choices presented in (23) do not satisfy conservative conditions (16). Nevertheless, synchronization is observed.

Self Induced Bursting. Increasing the timescale of diffusion by a factor of two ($k = 0.2$) leads to another interesting result (figure 7). Although the
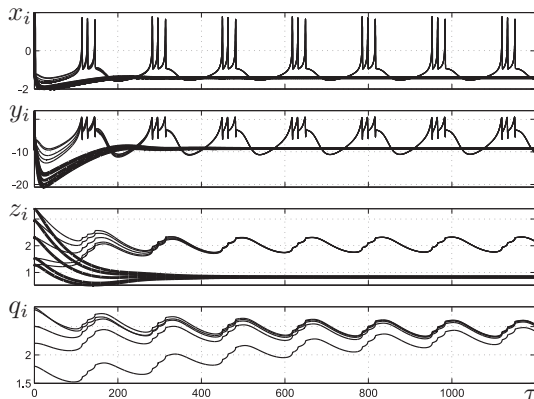
Fig. 7. Simulation results. Thin lines: extended model, 'self induced bursting'. Thick lines: original model.

parameters for both systems (extended and original model) are identical, figure 7 shows that the original model converges to a stable equilibrium, while the modified model gives a bursting response. This response exists by virtue of the diffusive coupling in the modified system. In addition to providing an extra input from other neurons, diffusive coupling allows for self coupling. This 'self-excitation' exceeds the input by diffusion from any other neuron (11). Furthermore, the observed behaviour persists if a single neuron is simulated.

V. CONCLUSION

Concluding, we have presented a theoretical analysis of neuronal dynamics, taking spillover of neurotransmitter into account. First of all, we have shown the coupling function generated by diffusive coupling to follow the Gaussian law by analyzing hippocampal tissue of mice. Secondly, we have implemented this coupling in the Hindmarsh & Rose model and new types of dynamic behaviour were revealed, which can be specifically linked to the presence of diffusive coupling. Furthermore, the limiting behaviour of the new model has been investigated and a sufficient condition for global asymptotic stability of the synchronization manifold has been derived.

REFERENCES

[1] A. Lebedinskiy, V.B. Kanzantsev, and A.V. Semyanov. Extracellular diffuse signal formed by astrocytic network guides propagation of neuronal activity. In A. Semyanov, editor, *Proceedings of the Neuroscience Meeting*. Society for Neuroscience, 2006.

[2] A. Yu. Pogromsky. Passivity based design of synchronizing systems. *Int. J. of Bifurc. and Chaos*, 8(2):295–319, 1998.

[3] B. Demidovich. Lectures on stability theory (in russian), Nauka, Moscow, 1967.

[4] D.J. Rijlaarsdam. Qualitative modeling of neuronal behaviour (effects of diffusion). Technical Report DCT 2007.022, Eindhoven University of Technology, June 2007, available at: http://yp.wtb.tue.nl/pdfs/8091.pdf.

[5] H. Nishiyama and D. Linden. Pure spillover transmission between neurons. *Nature Neuroscience*, 10(6):675–676, June 2007.

[6] M. Heath. *Scientific Computing*. McGraw-Hill, 2002.

[7] I. Tyukin, E. Steur, H. Nijmeijer, and C. van Leeuwen. Non-uniform small-gain theorems for systems with unstable invariant sets. *SIAM Journal on Control and Optimization*. Accepted, preprint is available at http://arxiv.org/abs/math.DS/0612381.

[8] E. Izhikevich. Which model to use for cortical sipiking neurons? *IEEE Trans. on Neural Networks*, 15(5):1063–1070, September 2004.

[9] J. Dantzig and C. Tucker III. *Modeling in Materials processing*. Cambridge University Press, 2001.

[10] J.L. Hindmarsh and R.M. Rose. The assembly of ionic currents in a thalamic neuron. *Proc. R. Soc. Lond.*, B(237):267–288, 1989.

[11] A. Pavlov. *The output regulation problem: a vonvergent dynamics approach*. PhD thesis, Eindhoven University of Technology, October 2004.

[12] L. Savtchenko. Extracellular diffusity determines contribution of high-versus low-affinity receptors to neural signaling. *Neuroimage*, 25(1):101–111, March 2005.

[13] A. Semyanov. Diffusional extrasynaptic neurotransmission via glutamate and gaba. *Neurosci. Behav. Physiol.*, (35):253–266, March 2005. Review.

[14] O. Taussky. A recurring theorem on determinants. *The American Mathematical Monthly*, 56(10):672–676, December 1949.

[15] W. Oud, I. Tyukin, and H. Nijmeijer. Sufficient conditions for synchronization in an ensemble of hindmarsh and rose neurons: Passivity-based approach. *Proceedings NOLCOS 2004*, 2004.